RAPID COMMUNICATIONS

PHYSICAL REVIEW E VOLUME 53, NUMBER 1 JANUARY 1996

Dynamics of monopole annihilation by type-1/2 strings in a nematic liquid crystal

Andrew N. Pargellis,[1] John Mendez,[2] Mohan Srinivasarao,[3] and Bernard Yurke[1]
[1]*AT&T Bell Laboratories, Murray Hill, New Jersey 07974*
[2]*Colby College, Waterville, Maine 04901*
[3]*College of Textiles, North Carolina State University, Raleigh, North Carolina 27695*
(Received 24 August 1995)

In uniaxial nematic liquid crystals, monopoles can be annihilated by type-1/2 strings. We present experimental measurements on the dynamics of this process as well as others, including loop collapses and monopole-pair annihilations. On dimensional grounds one expects the size of a collapsing structure in a nematic liquid crystal to scale as $\tau^{1/2}$ where τ is the time to annihilation. Indeed, type-1/2 loops and monopole-antimonopole pairs exhibit this kind of behavior. In contrast, for monopole annihilation by a type-1/2 string we find that the string-monopole separation scales as τ^{α} where $\alpha = 0.629 \pm 0.006$.

PACS number(s): 61.30.Jf, 05.70.Ln, 64.70.Md

Recently, there has been considerable theoretical and experimental work directed at understanding annealing processes in systems whose topological defects are something other than domain walls [1]. Because they are amenable to experimental study, uniaxial nematic liquid crystals have received considerable attention in this regard [2–6]. Uniaxial nematic liquid crystals are particularly interesting in that they possess topological defects belonging to three different homotopy classes, that is, they possess stringlike defects, referred to as strings or type-1/2 disclination lines, pointlike topological defects, referred to as "hedgehogs" or monopoles, and nonsingular topological defects, referred to as "texture" defects [3,7]. The defect tangle produced by the quench of a uniaxial nematic liquid crystal material from the isotropic phase to the nematic phase possesses all these defect types although strings predominate. In the annealing process the correlation length, deduced from disclination line length [3–5] and light scattering measurements [6], has been observed to grow as $t^{1/2}$ where t is the time since the quench. For such a system to exhibit self-similar scaling one would expect the monopole density to decay as $t^{-3/2}$. In contrast, what has been observed [4] is that the monopole density grows at early times, reaches a peak, and then decays more rapidly than expected. To understand this behavior it is desirable to obtain a better understanding of how monopoles are created [8] and destroyed in defect tangles.

We have thus undertaken as experimental study of the annihilation process of a monopole by a string. This is the dominant mechanism by which monopoles are removed from a defect tangle although monopole-antimonopole annihilation is also frequently seen [4]. From studies of loop collapse [3] and monopole-antimonopole annihilation [9–11] it has been seen that a collapsing defect structure enters a self-similar scaling regime in which the size of the defect structure scales as $\tau^{1/2}$ where τ is the time to collapse. Such behavior is expected on dimensional grounds from the form of the Ericksen-Leslie equations [12] that govern director-field reorientation. In contrast, the $\tau^{1/2}$ scaling is not observed for the measurements reported here on the time dependence of the distance between a monopole and a type-1/2 string. Instead, this distance decreases as $\tau^{0.63}$. To corroborate previous measurements, we have also measured, for the same liquid crystal material, the time dependence of loop and monopole-pair annihilation. In addition, we have measured the collapse of "apparition" loops and type-1/2 loops decorated with apparitions.

Besides the type-1/2 disclination lines other stringlike structures can be seen in uniaxial nematic liquid crystals when viewed via transmission microscopy without polarizers. These structures are not topological defects, however. Following previous literature [13] we refer to these as apparitions. The diffuse appearance of apparitions makes them easy to distinguish from the type-1/2 strings. Apparitions often appear to be associated with regions where the director field undergoes a winding of 1 and have thus been referred to as type-1 disclination lines. Apparitions are an imaging artifact of the way light is guided through a nonuniform director field. This is easily demonstrated by viewing a defect tangle from several directions, for example, by rotating a cylindrical capillary containing the defect tangle. In this case one finds that the apparitions often do not exhibit rigid body rotation while the strings and monopoles always do.

Examples of the five classes of defect structures whose collapse dynamics we have studied are shown in Fig. 1. Figure 1(a) depicts an isolated loop consisting of a type-1/2 string. Figure 1(b) depicts an isolated apparition loop. Apparition loops are rare; only two were observed during the course of collecting data from over 100 runs. Figure 1(c) shows a monopole-antimonopole pair on an apparition loop. Monopole-antimonopole pairs generally reside on apparition loops or apparition strings, the apparition loops being the most common. We have found no statistically significant difference in dynamics of monopole-antimonopole annihilation for the case when both are connected by an apparition line or both are connected by an apparition loop. Figure 1(d) shows a type-1/2 loop with two apparition lines extending from opposite sides of the loop. Upon collapse of type-1/2 loop decorated with a pair of apparition lines may or may not leave behind a monopole. For the liquid crystal K15 we have found that 25% of such structures generated from defect tangles produced by sudden pressure jumps result in monopoles [4]. In contrast, we have never seen an undecorated

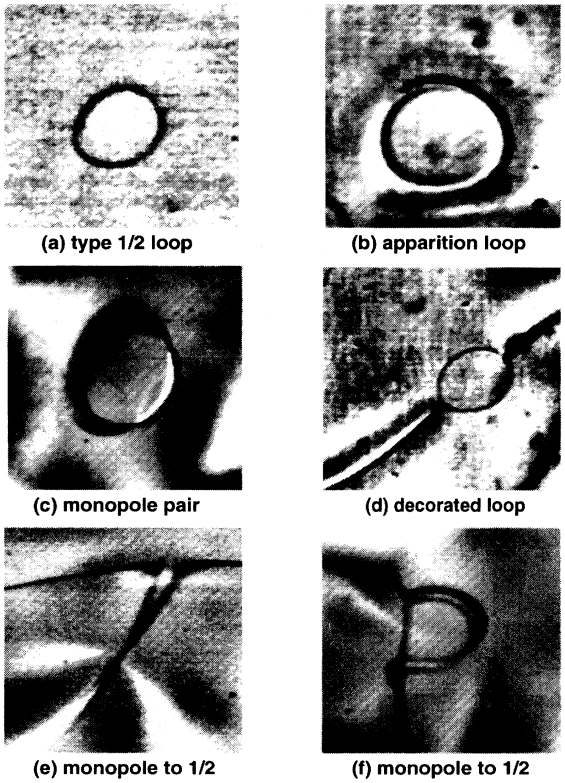

FIG. 1. Examples of the five classes of collapsing defect structures discussed in this study. These are representative of the images we processed for the collapse dynamics data. The full width is 530 μm for the images (a) and (c)–(f) and 350 μm for image (b). (a) Isolated type-1/2 loop; (b) isolated apparition loop; (c) monopole-antimonopole pair; (d) type-1/2 loop decorated with apparitions; (e) monopole and type-1/2 string connected via an apparition; (f) monopole and type-1/2 string connected via an apparition loop.

type-1/2 loop [such as that of Fig. 1(a)] produce a monopole upon collapse. Figures 1(e) and 1(f) show a monopole in the process of annihilation with a type-1/2 disclination line. In Fig. 1(e) the monopole is connected to the type-1/2 disclination line via an apparition. In Fig. 1(f) both ends of the apparition are attached to the type-1/2 string.

A uniaxial nematic liquid crystal, commercially known as E7, was used in the experiments reported here. This liquid crystal is a eutectic mixture of four cyanophenyls: 4-cyano-4′-*n*-pentylbiphenyl (K15), 4-cyano-4′-*n*-heptylbiphenyl (K21), 4-cyano-4′-*n*-octoxybiphenyl (M24), and 4-cyano-4″-*n*-pentyl-*p*-terphenyl (T15). The phase transitions occur at the following temperatures: isotropic-to-biphasic (60.1 °C), biphasic-to-nematic (58.3 °C), and nematic-to-solid (−10 °C). We chose this material because of the large biphasic region. During a temperature quench, nematic droplets nucleate in the biphasic region. Upon coalescence, these droplets yield a defect tangle rich in monopoles and, hence, rich in the kind of defect configurations we sought to study.

The sample cell has been described previously [14]. Briefly, a horizontally oriented wire loop, approximately 3 mm across, contains a film of the liquid crystal material. Electric current flowing through a resistive element attached to the wire loop provides heat to maintain the liquid at 70 °C,

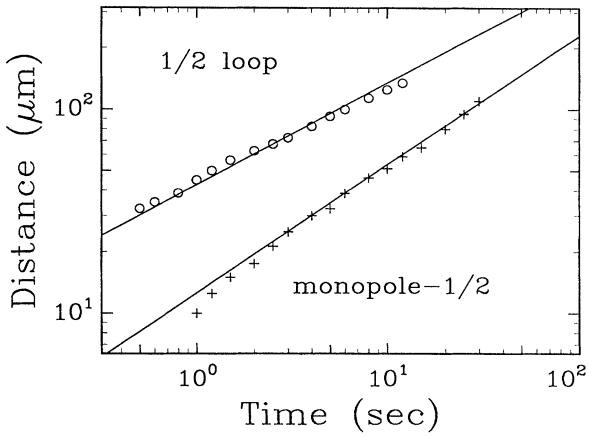

FIG. 2. Separation distance d versus time to collapse τ. The isolated type-1/2 loop data scales as $d \approx \tau^{-0.5}$ and the monopole approaching a type-1/2 string data scales as $d \approx \tau^{-0.63}$.

a temperature well into the isotropic phase. The sample is quenched to the nematic phase and maintained at room temperature simply by turning off the current to the resistive element. The sample cools through the transition temperature at a rate of 1.4 °C/s. The sample reaches a temperature of 28 °C in 100 s and then decreases another 3 or 4 °C over the next several hundred seconds, during which period the data for the collapse of defect structures are taken. The film was observed with optical microscopy in transmission at low magnification and the microscope images were recorded with the HSV-400 high-speed color video recorder (NAC, Inc.) at a rate of 200 frames/s. The separation distances of defects were then measured from the video frames with an accuracy of ± 1.25 μm. The film was typically 400 μm thick and care was taken to ensure that the defects under observation were within 50 μm of the film center to minimize the influence of surface effects on the observed dynamics [14]. A further criterion for study was that a defect structure with a characteristic size d had to be at least a distance $1.5d$ from all neighboring defects.

Data on the time dependence of a characteristic dimension d of a collapsing defect structure were fit to the form

$$d(t) = A\tau^{\alpha} \tag{1}$$

where $\tau = t_0 - t$ is the time to collapse, t_0 is the time of collapse, and t is time. This functional form was motivated by previous observations that collapsing defect structures enter a self-similar scaling regime. All three parameters (α, A, and t_0) were extracted through a least squares fit of the size versus time data taken from the video images.

Figure 2 shows representative data for the annihilation, as a function of time, of an isolated type-1/2 loop and also of a monopole being annihilated by a type-1/2 disclination line. For the loop, the distance d is taken to be the diameter along the major axis. For the monopole annihilation by a type-1/2 disclination line, d is the shortest distance between the monopole and the disclination line. The solid line through the loop data has a $\tau^{1/2}$ time dependence. The line drawn through the monopole-type-1/2 line has a $t^{0.63}$ time dependence.

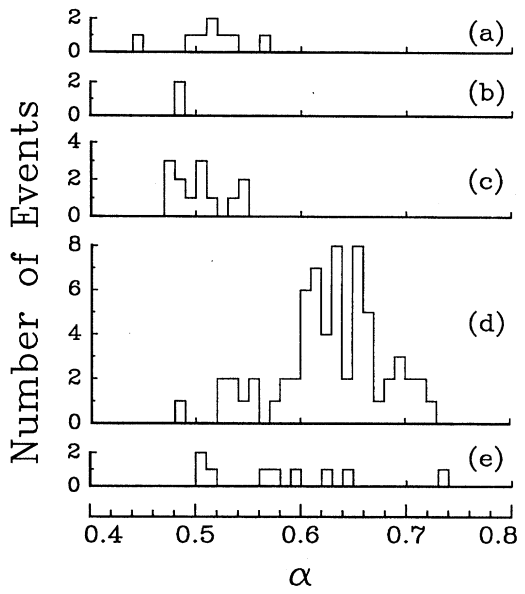

FIG. 3. Number of events as a function of scaling exponent α for the five events discussed in this work. (a) Isolated type-1/2 loop collapse; (b) isolated apparition loop collapse; (c) monopole pair annihilation; (d) monopole annihilation on a type-1/2 string; (e) apparition decorated type-1/2 loop collapse.

The distribution of scaling exponents α is shown in Fig. 3 for the five different classes of events discussed. The runs for each class are binned in α, each bin being 0.05 wide as shown on the horizontal scale at the bottom of the figure. The first three classes all exhibit behavior consistent with $d \sim t^{-1/2}$ scaling. The fourth class, monopole annihilation by a type-1/2 string, shows the values of α to be peaked about 0.63, a value significantly greater than 0.5. The fifth and final class, type-1/2 loop with apparitions, shows a large dispersion in the measured scaling exponents.

The number of events of a given type of defect configuration, together with the mean value of α and its standard deviation $\Delta\alpha$, and the mean value of A and its standard deviation ΔA, are given in Table I. The entries for α also give its statistical uncertainty. For the case of monopole-antimonopole annihilation, d was chosen to be the distance between the two monopoles. The values of α listed are the average of the values obtained by a full fit of Eq. (1). The values of α for isolated type-1/2 loops, isolated apparition loops, and monopole-antimonopole pairs are consistent with $\alpha = 1/2$. This is consistent with previous observations of type-1/2 loop collapse [3,4] and monopole-antimonopole annihilation [9]. The scaling of the distance between a monopole and a type-1/2 string is, however, not consistent with $\alpha = 1/2$, as is evident both from the Table I entries and histogram plot of Fig. 3. Effects which would systematically modify the motion of the defects, such as dirt trapped on the defects, would influence the dynamics of type-1/2 loop collapse or monopole-antimonopole annihilation. The fact that the data are consistent with $\alpha = 1/2$ for type-1/2 loop collapse data and monopole-antimonopole annihilation data argues strongly that the exponent $\alpha = 0.629 \pm 0.006$ measured for the case of a monopole merging with a type-1/2 string is not the result of systematic measurement errors or dirt effects. In addition, the standard deviation in α is roughly twice as large for a monopole merging with a string than it is for type-1/2 loop collapse and monopole-antimonopole annihilation. This indicates that there is something intrinsically noisy about the monopole-string merger process. We have separately analyzed the data for the two types of monopole-string configurations shown in Fig. 1(e) and Fig. 1(f). We find no statistically significant difference in the measured α and A for these two configurations. Even greater dispersion is exhibited in the dynamics of type-1/2 loops decorated with apparitions, as seen from Table. I.

Since the measured values of α obtained for type-1/2 loops, apparition loops, and monopole-antimonopole pairs are consistent with 1/2, a second fitting procedure was used for these cases by constraining α to be 1/2. It is the average of these values of A that are listed in Table I. However, these values vary by less than 5% from those that were obtained by a full fit. Since the α obtained for monopoles merging with type-1/2 strings and the collapse of type-1/2 loops with apparitions is not consistent with $\alpha = 1/2$, the average value A reported in Table I for these entries is that obtained by performing a full fit to Eq. (1) with α unconstrained.

The theory for the values of A is still at a rudimentary stage, but presumably A depends on the splay, twist, and bend elastic constants (K_{11}, K_{22}, and K_{33}, respectively) and on the reorientational viscosity γ_1. We have argued, for the cases of loop collapse [3,4] and monopole-antimonopole annihilation [9], that for the equal elastic constant case, $K = K_{11} = K_{22} = K_{33}$, A has the form

$$A = g(K/\gamma_1)^{1/2}, \tag{2}$$

TABLE I. Defect collapse parameters obtained by fitting the data to $d = A(t_0 - t)^{\alpha}$. The values of A listed are those obtained when d has units of micrometers and t has units of seconds. The values of A quoted for the type-1/2 loop, the apparition loop, and the monopole-antimonopole were obtained through fits of the data for which α was constrained to be 1/2.

Configuration	Number of events	α	$\Delta\alpha$	A	ΔA
type-1/2 loop	8	0.514 ± 0.013	0.035	44.4	4.9
apparition loop	2	0.488		37.1	7.2
monopole-antimonopole	15	0.505 ± 0.006	0.024	19.5	3.2
monopole and type-1/2 string	64	0.629 ± 0.006	0.050	10.1	3.5
type-1/2 loop with apparitions	9	0.584 ± 0.027	0.075	33.2	9.3

where g is a geometrical factor that depends on the defect configuration. For the case of monopole-antimonopole annihilation, it has been determined from numerical studies [9] that $g=1.68\pm0.07$. We have obtained an experimental value for g for the case of loop collapse in K15 liquid crystal material. For K15 the twist elastic constant K_{22} is smaller by roughly a factor of 2 than the other elastic constants. It is thus reasonable to assume that a collapsing type-1/2 loop in this material consists primarily of a twist disclination loop. In this case one would expect that the appropriate form of A would be that given in Eq. (2) with K replaced by K_{22}. For loop collapse in K15 at 25 °C we measure $A=33.9\pm1.5$ μm s$^{-1/2}$. Using Eq. (2) and the measured values for K15 at 25 °C, K_{22}(K15)=6.0 pN [15] and γ_1(K15)=0.087 Pa s [16], one obtains $g=4.10\pm0.20$ for a collapsing loop. Taking the ratio of the experimentally determined value of g for loop collapse to the theoretical value for monopole-antimonopole annihilation one obtains, for the equal constant case, $g_l/g_m=A_l/A_m=2.44$ where the subscripts l and m indicate the g and A values for loops and monopoles, respectively.

Values of the elastic constants for E7 as a function of temperature have been published [17]. For the temperature 25 ± 1 °C at which our experiments were carried out they are $K_{11}=10.6$, $K_{22}=10.4$, and $K_{33}=20.5$ pN. Thus, the equal constant approximation for A_l/A_m may be adequate. From Table I, one obtains $A_l/A_m=2.26$ which is within 10% of the value 2.44 we had argued for in the previous paragraph [18]. Also, using the experimentally determined value of g for the case of loop collapse, Eq. (2), and our experimentally determined A_l, one calculates that $\gamma_1/K_{22}=8.53\pm2.8$ ms μm^{-2}.

The literature value for the rotational viscosity at our temperature [16] has the value $\gamma_1-0.21$ Pa s. Therefore, the value for γ_1/K_{22} extracted from the literature is 20.2 ms/μm^2. The value of γ_1/K_{22} we have determined from loop collapse data is within about a factor of 2 of this value. This indicates that measurement of the collapse dynamics of defect structures may provide a convenient way of measuring the γ_1/K_{ii} provided the theory for the A coefficients is improved.

A theoretical understanding of α and A for the case of monopole annihilation on a string has yet to be obtained. One expects that, as the monopole approaches the string, asymptotic behavior, insensitive to the director field at large distances, should appear. This is consistent with our observations that the string-monopole separation does scale as indicated by Eq. (1), although its exponent is closer to 5/8 than 1/2. The influence of the boundaries, the ability of a monopole to transform itself from one type to another through global rotations of the director field, and the fact that in the unequal constant case different types of monopoles have different energies, may account for the greater variance in α and A seen in the data for the merging of a monopole with a type-1/2 string.

We gratefully acknowledge useful discussions on the material properties of liquid crystals with Frank V. Allan.

[1] A. J. Bray, Adv. Phys. **43**, 357 (1994); R. E. Blundell and A. J. Bray, Phys. Rev. A **46**, R6154 (1992).

[2] M. J. Bowick, L. Chandar, E. A. Schiff, and A. M. Srivastava, Science **263**, 943 (1994).

[3] I. Chuang *et al.*, Science **251**, 1336 (1991); I. Chuang, N. Turok, and B. Yurke, Phys. Rev. Lett. **66**, 2472 (1991).

[4] I. Chuang *et al.*, Phys. Rev. E **47**, 3343 (1993); B. Yurke, A. N. Pargellis, I. Chuang, and N. Turok, Physica B **178**, 56 (1992).

[5] R. Snyder *et al.*, Phys. Rev. A **45**, R2169 (1992); B. Yurke, A. N. Pargellis, and N. Turok, Mol. Cryst. Liq. Cryst. **222**, 195 (1992).

[6] A. P. Y. Wong, P. Wiltzius, and B. Yurke, Phys. Rev. Lett. **68**, 3583 (1992); A. P. Y. Wong *et al.*, Phys. Rev. E **47**, 2683 (1993).

[7] N. D. Mermin, Rev. Mod. Phys. **51**, 591 (1979); M. Kleman, in *Advances in Liquid Crystals*, edited by G. H. Brown (Academic, New York, 1975), Vol. 1.

[8] M. Hindmarsh, Phys. Rev. Lett. **75**, 2502 (1995).

[9] A. Pargellis, N. Turok, and B. Yurke, Phys. Rev. Lett. **67**, 1570 (1991).

[10] O. D. Lavrentovich and S. S. Rozhkov, Pis'ma Zh. Éksp. Teor. Fiz. **47**, 210 (1988) [JETP Lett. **47**, 254 (1988)].

[11] A. Rapini, L. Leger, and A. Martinet, J. Phys. (Paris) Colloq. **36**, C1-189 (1989).

[12] P. G. de Gennes, *The Physics of Liquid Crystals* (Oxford University Press, London, 1974); S. Chandrasekhar, *Liquid Crystals* (Cambridge University Press, Cambridge, England 1992).

[13] C. E. Williams, P. E. Cladis, and M. Kleman, Mol. Cryst. Liq. Cryst. **21**, 355 (1973).

[14] A. N. Pargellis *et al.*, Phys. Rev. A **46**, 7765 (1992).

[15] P. P. Karat and M. V. Madhusadana, Mol. Cryst. Liq. Cryst. **40**, 239 (1977).

[16] S.-T. Wu and C-S. Wu, Phys. Rev. A **42**, 2219 (1990).

[17] M. Schadt and F. Müller, IEEE Trans. Electron. Devices **ED-25**, 1125 (1978).

[18] The agreement may be somewhat fortuitous since major inconsistencies exist in literature regarding the γ_1, K_{ii}, and their ratios. For example, S-T. Wu and R. J. Cox, in J. Appl. Phys. **64**, 82 (1988), report that at 25 °C for K15 (5CB), $\gamma_1/K_{11}=13.5$ ms/μm^{-2} which is almost a factor of 2 greater than that computed from Refs. [15,16].

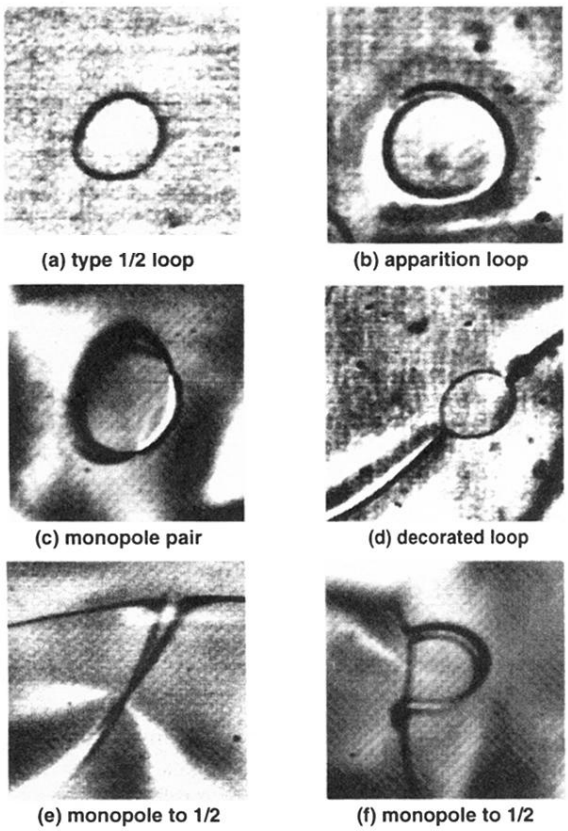

FIG. 1. Examples of the five classes of collapsing defect structures discussed in this study. These are representative of the images we processed for the collapse dynamics data. The full width is 530 μm for the images (a) and (c)–(f) and 350 μm for image (b). (a) Isolated type-1/2 loop; (b) isolated apparition loop; (c) monopole-antimonopole pair; (d) type-1/2 loop decorated with apparitions; (e) monopole and type-1/2 string connected via an apparition; (f) monopole and type-1/2 string connected via an apparition loop.